HiSST: 3rd International Conference on
High-Speed Vehicle Science Technology
14 -19 April 2024, Busan, Korea

Experimental Investigation of the Global Equivalence Ratio Influence in a Hydrogen-fueled Supersonic Combustor

E.S. de Souza[1,2], L.A.G. Ribeiro[1], L.M. Vialta[1], P.A.S. Matos[1], L.G. Barreta[1], G.P. Camillo, I.S. Rêgo, L. Galembeck[1], D. Carinhana Jr[1], and P.T. Lacava[2]

Abstract

The relation between the spatial pressure profile and global equivalence ratio is investigated in a hydrogen-fueled supersonic combustor directly connected to a shock tunnel facility. The combustor model comprises an initial constant area section (isolator), followed by a single-hole fuel injection point, a flame-holder cavity, and finally, an expansion ramp. The results are obtained for a freestream inlet flow at Mach 2.7, calculated static temperature of 705 K, and static pressure of 164 kPa, with stagnation conditions at 1,470 K and 3.8 MPa. The global equivalence ratio (φ_G) ranged from 0.10 to 0.50. The pressure variation resulting from combustion was measured using dynamic pressure transducers installed along the model. Experimental data are compared to an idealized model for adiabatic constant-volume combustion, showing a direct correlation between combustion pressure ratio and fuel mass flow rate. The experimental results demonstrate a linear relationship for global equivalence ratios φ_G below approximately 0.25, indicating a combustion dynamic with linear dependency on φ_G. As it increases, the flow dynamics exhibit reduced sensitivity to changes in φ_G, posing a challenge for predictive modeling.

Keywords: *supersonic combustion, scramjet combustor, equivalence ratio, flameholder, shock tunnel*

Nomenclature

Latin
A – Area
A^* – Throat area of the nozzle
$\dot{m}$ – Mass flow
p – Pressure
R – Gas constant
S – Sensor
T – Temperature
U – Velocity
Greek
γ – Ratio of specific heats
φ – Equivalence ratio

Subscripts
G – Global
i – Injection
p – Related to the plenum
PS – Primary shock
S – Related to the free-stream
0 – Related to the total conditions
1 – Related to the driven
2 – Related to the shocked conditions
4 – Related to the driver
5 – Related to the stagnation conditions

[1] *Institute for Advanced Studies and Aeronautics Institute of Technology, Brazil, schiavinatoess@fab.mil.br*
[2] *Institute for Advanced Studies, São José dos Campos, Brazil, lucaslagr@fab.mil.br*
[3] *Institute for Advanced Studies, São José dos Campos, Brazil, ledavialta0@gmail.com*
[4] *Institute for Advanced Studies, São José dos Campos, Brazil, pedrosmatos@gmail.com*
[5] *Institute for Advanced Studies, São José dos Campos, Brazil, barreta2@gmail.com*
[6] *Institute for Advanced Studies, São José dos Campos,* Brazil, *gianninocamillo@gmail.com*
[7] *Institute for Advanced Studies, São José dos Campos,* Brazil, *israelisr@fab.mil.br*
[8] *Institute for Advanced Studies, São José dos Campos,* Brazil, *galembeckIq@fab.mil.br*
[9] *Institute for Advanced Studies, São José dos Campos,* Brazil, *dermevaldcj@fab.mil.br*
[10] *Aeronautics Institute of Technology, São José dos Campos,* Brazil, *pedrotlacavaptl@fab.mil.br*

1. Introduction

Over the past decades, SCRamjet engines have received significant attention due to their importance in the development of hypersonic systems. Since the idea of adding heat to supersonic flow was first explored in the 1940's [1], numerous research programs have aimed at the development of hypersonic airbreathing propulsion systems [2]. This type of system requires stable combustion reactions within the engine to achieve reliable thrust and high propulsion efficiency over a wide range of flight conditions [3]. Consequently, it is critical to better understand the physical and chemical mechanisms involved in the process to improve this technology. [4]. In this context, there are several challenges that must be overcome to achieve full maturity in the development of SCRamjets, with some of these challenges being directly associated with supersonic combustion itself. Some of these key parameters for understanding supersonic combustion are the improvement of the air-fuel mixture and the equivalence ratio, which can be directly related to the heat release rate [5].

Given that the airflow within a SCRamjet is supersonic, it is essential that the mixing of air and fuel takes place within a short duration. With the aim of optimizing the energy deposited in the combustion chamber, a variety of internal structures have been proposed for the purpose of facilitating mixing and flame anchoring. In general, such structures are based on the generation of distinct low-speed regions that are kinetically favorable for stabilizing and sustaining the combustion reaction [6]. The total pressure losses along the combustor significantly diminish the engine's performance, necessitating that mixing structures exert minimal impact on the supersonic flow. From this perspective, wall-inserted cavities have proven to be an efficient means of flame anchoring in SCRamjet engines [7,8,9,10], as they induce flow and combustion gas recirculation, reducing flow velocity, increasing fuel residence time, and promoting the mixing and combustion of reactants [7]. The efficiency of the cavities, concerning mixing capability and flame stabilization, primarily depends on their geometry and the position of the fuel injectors. The cavity geometry directly influences the size of the recirculation zone and the development of the shear layer, resulting in different flame behaviors during the ignition process [11]. Therefore, although the cavity flameholder usually has a very simple geometry, the flow and combustion mechanisms involved are quite complicated [12].

Regarding the global equivalence ratio, it has a direct impact on the flow field, mixing and supersonic combustion characteristics [13]. The turbulence level within the environment is influenced by the pressure of fuel injection, thereby impacting the mixing time. The increase in fuel caused by the rise in pressure can lead to changes in the distribution of the fuel/oxidizer pair, which, in turn, alters the burning velocity distribution and thus the reaction time. Therefore, by varying the equivalence ratio values, it is possible to study such effects.

To experimentally investigate the influence of the global equivalence ratio on combustion pressures, a supersonic combustor model equipped with a cavity flameholder was tested in a shock tunnel, operating in the direct-connect model. A series of experiments were carried out using the same freestream flow conditions at the model entrance, with a range of hydrogen injection pressures, leading to an φ_G spanning from 0.10 to 0.50.

2. Material and Methods

The experiments were conducted in the T1 shock tunnel, located at the Hypersonic and Aerothermodynamics Laboratory (LAH) of the Institute of Advanced Studies (IEAv). The T1 device is directly connected to a combustion chamber for supersonic combustion studies. In this paper, the shock tube term refers to the portion of the T1 shock tunnel that comprehends the driver and driven sections. The shock tunnel nozzle and test section, that comprehend the combustion chamber and the injection system, otherwise, are referred as combustor.

2.1. Shock Tube

The shock tube conditions were kept constant in all experiments. The driver and driven sections were separated by a double diaphragm system (DDS) and were filled with helium at 6 MPa and air at 50 kPa.

This configuration provided total temperature of 1470 K and pressure of 3.8 MPa. Along the driven tube, 5 dynamic pressure transducers were installed for experiment characterization. These sensors are used to record the primary shock speed (U_{ps}), air-flow shocked pressure (p_2), and the total air pressure (p_0). These parameters are used for complete estimation of the air-flow total conditions and to ensure the T1 repeatability.

2.2. Combustor

At the end of the shock-tube driven, a geometry designed to embrace a contoured nozzle, an isolator and a combustion chamber was coupled. The nozzle produced a flow of Mach 2.7 at the isolator and is followed by the combustion chamber, including a 1.9 mm diameter orifice for transversal injection of molecular hydrogen (H_2), a cavity with dimensions of 20 mm width and 10 mm height, and finally, a 4° inclined expansion ramp. Nine PCB dynamic pressure sensors were installed on the upper wall (S1-S9) of the geometry. While the sensor S1 was positioned to characterize the free flow at the nozzle exit, the sensors from S2 to S9 were installed to measure the effects of H_2 injection.

Fig. 1 presents a schematic diagram with the nomenclature used for the sensors. The selected cavity was the one that demonstrated the best results in a previous work [14], in terms of flame anchoring and stability.

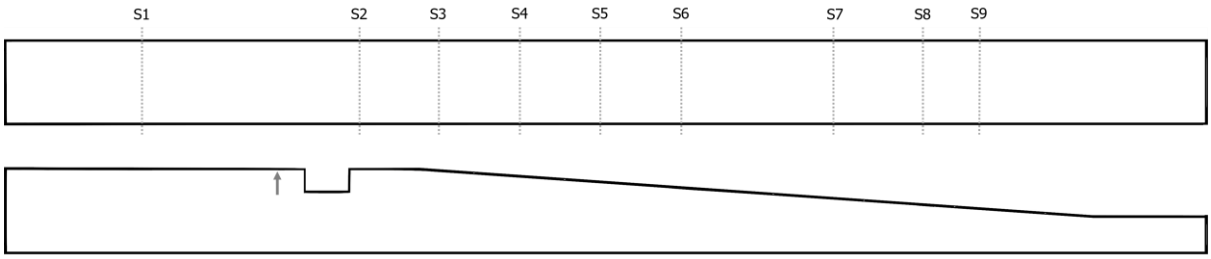

Fig. 1. Schematic diagram of the tested combustor model and the position of the pressure sensors (S1-S9) and injection (represented by an arrow).

A synchronization system was used to control the timing between the shock tunnel shot and fuel injection. Due to fluctuations in the DDS bursting process, injection occurred 100 to 200 ms prior to the arrival of air flow. The injection was started by a fast-acting valve, and an additional pressure transducer was positioned in the plenum upstream of the injection orifice for monitoring injection pressure and H_2 flow rates ($\dot{m}_{H2}$). As the injector geometry is fixed, considering a choked flow through the orifice and the plenum at room temperature (T_p), the amount of injected hydrogen is directly proportional to the plenum pressure (p_p), as stated in (1.

$$\dot{m_{H2}} = A_i \times \frac{p_p}{\sqrt{T_p}} \sqrt{\frac{\gamma}{R}\left(\frac{2}{\gamma+1}\right)^{(\gamma+1)/(\gamma-1)}} \tag{1}$$

where A_i, γ and R are, respectively, the injection orifice area, the ratio of specific heats and the gas constant for molecular hydrogen.

From the shock tube configurations, the combustion chamber air mass flow rate ($\dot{m}_{air}$) is calculated and was kept approximately constant in the experiments. From the plenum pressure, the fuel mass flow rate can be calculated from (1. Thus, a global equivalence ration can be φ_G defined and is calculated

by (2 [15]. This nomenclature is used to prevent ambiguity with the term common-sense equivalence ratio, well-established in premixed flames.

$$\varphi_G = 34.48 \frac{\dot{m}_{H2}}{\dot{m}_{air}} \quad (2)$$

Additional experiments without injection and with helium injection were used as references, providing insight into the flow dynamics along the combustor in the absence of combustion. Helium injection was conducted at the same injection pressures as hydrogen, allowing for the assessment of the injection pressure's influence on the established free-stream flow behavior.

Furthermore, the supersonic combustion results were compared with results from a constant volume combustion. The simplified 0D reactor assumes a homogeneous mixture of air/H_2 that reaches thermodynamic equilibrium at constant volume.

3. Results

A total of 32 experiments were conducted under the same shock tunnel setup and combustion chamber geometry, resulting in similar air-flow total conditions across all tests (see Table 1). The varying parameters were the gas injected into the supersonic flow at the combustion chamber and its injection pressure.

The supersonic combustion was fueled by molecular hydrogen, H_2, with injection pressure ranging from 0.5 to 2.5 MPa for a total of 20 tests, corresponding to a global equivalence ratio, φ_G, ranging approximately from 0.1 to 0.5. To isolate the exclusive effects of injection on the pressure field, as the generation of shock waves, 11 experiments were conducted with injection of Helium, with pressure injection ranging from 0.2 to 1.5 MPa. Finally, one test was performed without any injection to account for the cavity effects and resulted in the pressure profile basis.

Throughout this section, the results are separated by shock tunnel location – shock tube and test section - and by nature including injection pressures, definition of the reference pressure profile, combustion pressure profiles and an idealized pressure ratio.

3.1. Shock Tube

Pressure sensors installed along the driven tube provided measurements of primary shock speed, air-flow shocked pressure and total pressure. The results from all the experiments are summarized in the Table 1. As shown, the maximum coefficient of variation CoV was of 7.2% for the shocked pressure. However, the measured total pressure CoV was under 4%.

An in-house code was used to estimate the reflected condition from p_2 and U_{ps}, that is followed by an isentropic compression to the measured total pressure, assuming a thermally perfect air gas; the calculated total condition can be seen in Table 1.

Table 1. Measured and calculated shock tube conditions.

Shock Tube Parameters			
Measured		**Calculated**	
Primary Shock U_{ps}, m/s	1101 ± 34 (3,1%)	Total Temperature T_0, K	1470 ± 57 (3.9%)
Primary Shock Mach Number M_{ps}	3.2 ± 0.1 (3.1%)	Total Enthalpy h_0, MJ/kg	1.33 ± 0.07 (5.1%)
Shocked Pressure p_2, kPa	635 ± 46 (7.2%)	Total Density ρ_0, kg/m^3	0.81 ± 0.04 (5.5%)
Total Pressure p_0, MPa	3.81 ± 0.2 (3.8%)		

From the calculated total properties, the conditions of the air-flow freestream at the injection combustor entrance can be estimated by assuming a frozen isentropic flow through the nozzle for a nozzle-to-throat area ratio, A/A^*, of 3.5. This procedure leads to the results shown in Table 2.

Table 2. Calculated conditions at the injection position.

Combustion Chamber Parameters	
Calculated	
Velocity, m/s	1,376 ± 25 (1.8%)
Mach Number	2.67± 0.01 (0.3%)
Temperature, K	704 ± 28 (4.0%)
Static Pressure p_s, kPa	165 ± 10 (6.0%)
Normalized Pressure $p_s/p_0 \times 10^3$	43.1 ± 0.1 (0.2%)

3.2. Test Section: Combustion Chamber

All the pressure data from the combustion chamber section are presented in this section, categorized by injection pressure, reference pressure and combustion pressure. Unfortunately, instabilities on the second sensor, S2, positioned 3.7 cm downstream the injection, led to signal saturation and were not used in this work. Therefore, a total of eight wall pressure sensor were used to characterize the supersonic combustion, and an additional sensor at the injection plenum was used to calculate the fuel mass flow rate.

Additionally, all the wall static pressure measurements were normalized with respect to their corresponding total pressure. This procedure allows for proper comparison among the experiments by reducing the effects of the facility variability.

3.2.1. Injection Pressure

In Fig. 2. Injection pressures for all the experiments are displayed, except for the special case without injection. In the left plot, the injection pressure for the H_2 case ranges from 0.5 to approximately 2.5 MPa, indicated by red points. The Helium case is represented by blue squares. Error bars, although included, were smaller than the individual data points. The injection pressure was calculated based on the measured plenum pressure, which are plotted in the right figure against the global equivalence ratio, calculated by (1).

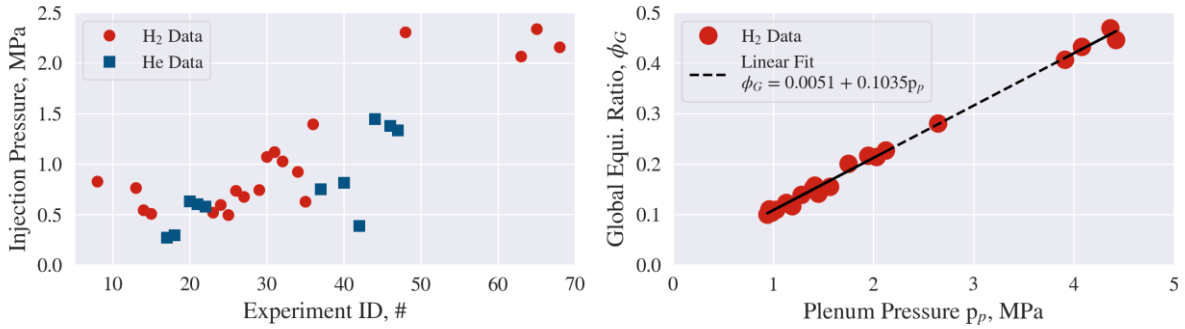

Fig. 2. Left: the injection pressure for each experiment and colored by injection gas, blue squares for Helium and red points for H_2. Right: the calculated global equivalence ratio for each experiment.

3.2.2. Reference Pressure Profile

In this section, a combustion-free pressure profile is obtained and defined as the pressure reference. This reference is used in the next section to quantify the combustion effects.

All the measured normalized pressure from the Helium and No-Injection cases are show in Fig. 3, where darker blue tones were used to represent higher injection pressures, p_i, and the black line the case without injection. Lines were drawn for the sole purpose of guiding the eyes. The figure includes a schematic representation of the combustion chamber and highlights the cavity positions and the sensors labels, all positioned relatively to the injection point. To enhance visualization of the data and their error bars, the original results were plotted with a slight horizontal shift.

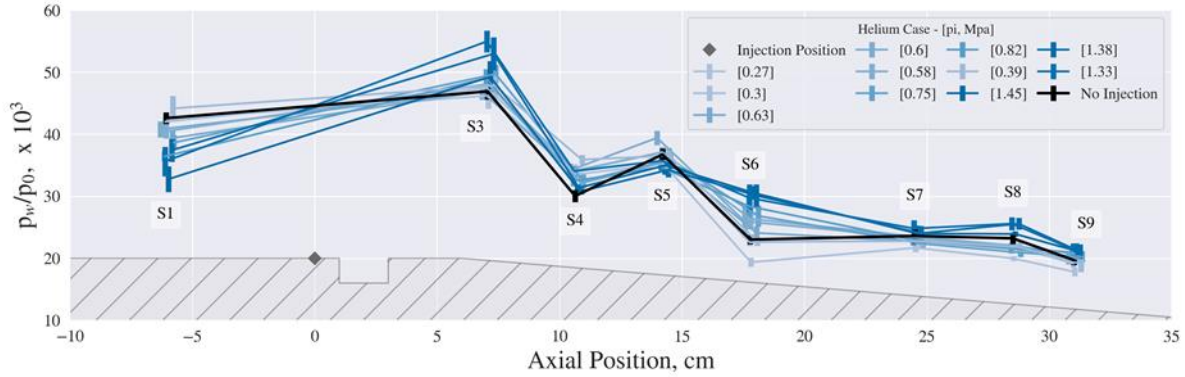

Fig. 3. Normalized Wall Pressures for the Helium and No-Injection cases. The sensors are sequentially labeled from S1 to S9.

From the Fig. 3, one can see the effects of injection of He are not negligible: for the sensors S1, S3 and S6, increasing the injection pressure leads to greater deviations from the No-Injection case. The observed increase in pressure on sensors downstream of the fuel injection location is expected as a direct effect of mass addition to the flow field. The more pronounced pressure increases on sensors S3 and S6, in opposition to a weaker effect in sensors S4 and S5, suggests the formation of a flow topology akin to a shock train. The significantly reduced discrepancies observed in the three most downstream sensors indicate that the length of the combustion chamber is such that it allows this shock train to dissipate, even in the cases of larger injection pressure. Looking now at sensor S1, Figure 3 shows that, upstream of the injection location, larger fuel injection pressures led to lower measured pressures in the combustion chamber. This is an unexpected effect, since Table 4 confirms that the experimental conditions generated by the shock tunnel had little variation between all runs. Furthermore, the measured pressures are consistently lower as the fuel injection pressure increases. One possible

explanation is a biasing of the piezoelectric pressure sensors due to an increase in back pressure before flow arrival in the tests, since the fuel injection valve is opened during the tunnel startup procedure, between 100 and 200 ms before steady-state conditions are achieved. Since these pressure sensors are differential with fast response, the slight and relatively slow change of back pressure moments before flow arrival would not be detected, but could modify the zero of the sensors, causing the observed effect.

From these results, the reference profile was defined as the mean pressure calculated sensor by sensor for the Helium case experiments to account for injection effects. The calculated reference can be seen in the Fig. 4.

3.2.3. Combustion Pressure Profile

In the same way as discussed in the previous section, the normalized wall pressures for the H_2 case were calculated and are plotted in the Fig. 4. For comparison purposes, the Helium and No-Injection cases are also displayed. The darker tones indicate higher injection pressure.

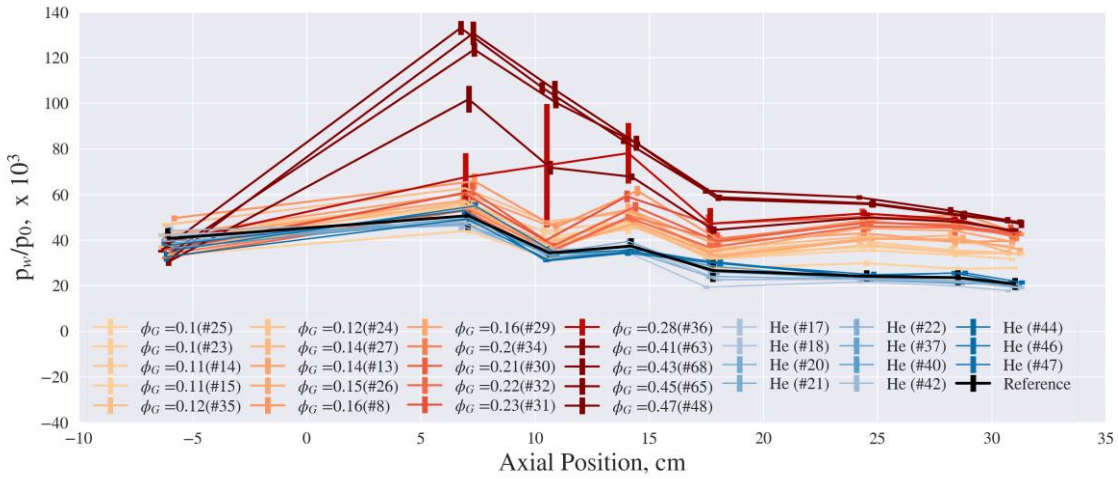

Fig. 4. Normalized pressure for all experiments. The injected gases are differentiated by the color of the plot, with blue representing He experiments and brown, H_2.

The normalized pressure data from the H_2 case were higher than the those from the Helium case for the sensors located after the injection, indicating supersonic combustion. For the low to intermediate global equivalence ratios, up to 0.25, combustion resulted in a low to moderate pressure increase, maintaining an approximately constant pressure along the combustor. In the cases of φ_G exceeded 0.28, the combustion induced to a significant pressure increase just after the injection. However, the final pressure levels were similar to those of globally leaner flame cases.

Initially, the rapid pressure increase noted in experiment #36 (φ_G = 0.28, p_i = 1.4 MPa) was attributed to the direct interaction between freestream and injection pressure. Though, the experiments with injection of helium did not exhibit the same behavior, even when the injection pressure was up to 1.45 MPa. Still, for experiments where H_2 injection pressures exceeded 1.45 MPa, there were no corresponding scenario in the set of helium experiments, making it difficult to quantify the injection effects.

High hydrogen injection pressures and consequent combustion are factors that can induce flow to thermal shock or boundary layer separation. In both possible scenarios, local pressure would experience a sudden increase as seen in Figure 4. The first case would also lead to 1) a reduction of the local Mach number to subsonic values and 2) an increase in pressure at sensors located upstream of the injection position. This alternative is rejected since 1) the reduction in wall static pressure observed in the figure

indicates the expansion process, resulting from supersonic flow and 2) the pressure measurements for sensor S1 are coherent across all experiments.

According to Korkegi [16], a pressure increase from p' to p" is sufficient to induce boundary layer separation if p"/p' is greater than 0.3 Ms2, an empirical criterion stated by the author for M_s lower than 4.5. In this paper, with a M_s value of 2.67, the ratio pressure of 2.15 is enough to separate the boundary layer and potentially compress the freestream to higher pressure values. Fig. 4 and Fig. 5 show that combustion experiments conducted with injection pressures exceeding 1.4 MPa (φ_G = 0.28) resulted in pressure ratios S3/S1 close to the calculated limit, suggesting the separation of boundary layer.

3.2.4. Pressure Ratio

Fig. 5 shows static wall pressure ratio calculated for the twenty experiments realized with H_2 injection, adopting the reference pressure profile as discussed in section 3.2.2. As can be notice, the injection of hydrogen gas increased chamber pressure above the reference level, indicating supersonic combustion.

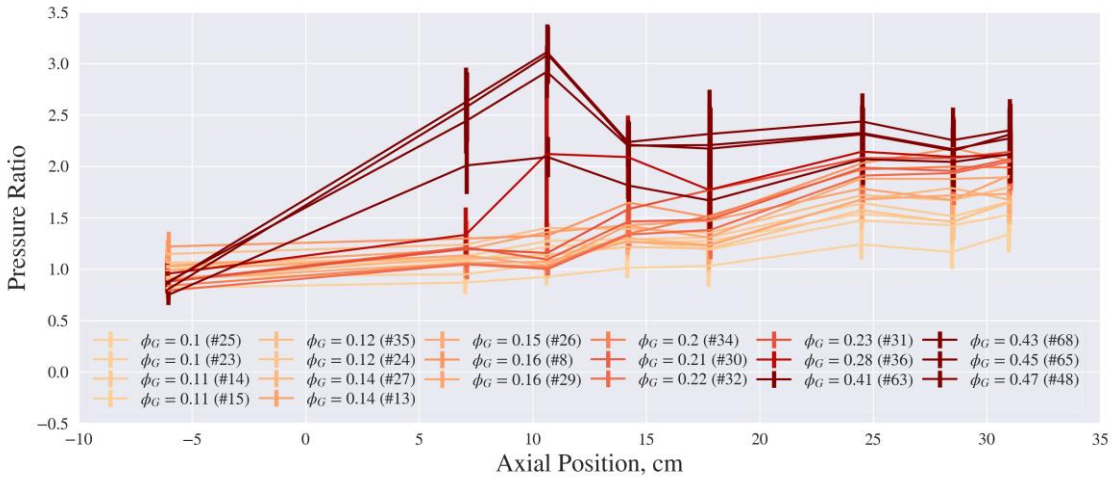

Fig. 5. Measured pressure ratio along the combustor; darker tones indicate higher injection pressure.

The results obtained for φ_G ranging from 0.1 to 0.28 show a pressure ratio profile increasing until an approximately constant value is reached at the three most downstream sensors. This observation suggests the characteristic flow transport time is comparable to the characteristic ignition time of the system, theoretically limited by both the reaction rate and the mixing rate.

For φ_G greater than 0.28, the figure displays pressure ratios of up to 3, surpassing those calculated theoretically under the assumption of adiabatic combustion in a closed volume. This result suggests an exaggerated compression of the flow, likely attributable to boundary layer separation, as discussed in the preceding section.

3.3. Pressure Comparison

The pressure ratio results obtained for the three most downstream sensors are compared with the idealized model of 0-dimensional adiabatic constant-volume combustion. Chemical equilibrium product was calculated by using the Cantera computational suite. Input data included a homogeneous and thermally perfect mixture of H_2/air with an equivalence ratio φ_G, reactant pressure given by the mean pressure registered by the sensor S1, and initial temperature given by the calculated local mean freestream temperature presented in Table 2. The pressure ratio is then defined as the ratio of product pressure to reactant pressure. It is important to note that under the assumption of a thermally perfect gas the calculated pressure ratio is virtually unaffected by changes in the pressure of the reactants.

Fig. 6 illustrates the comparison between experimental data from sensors S7, S8, and S9, and calculated results, with horizontal shifts to a better visualization. In gray, the figure depicts a region representing the calculated pressure ratios for reactant temperatures ranging from 676 to 732 K (± 1 standard deviation).

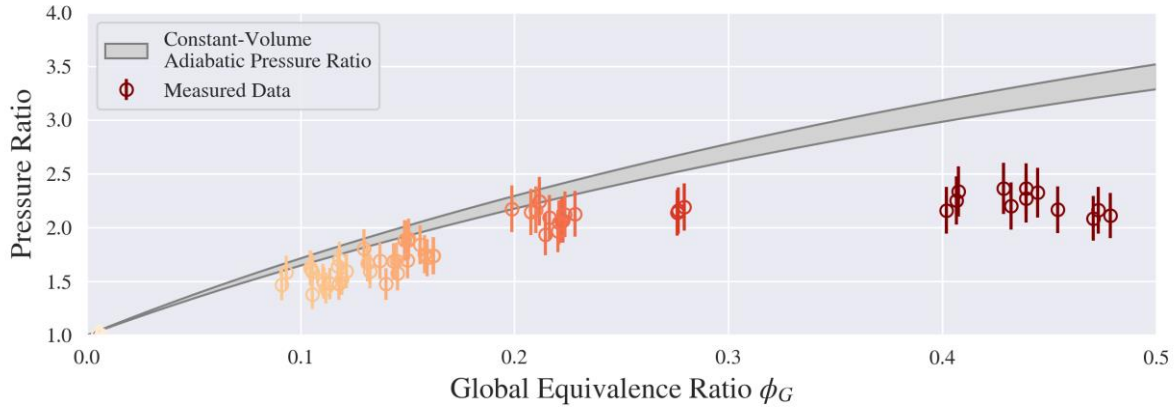

Fig. 6. Combustion pressure ratio as a function of global equivalence ratio.

For φ_G less than 0.25, the results show a strong linear correlation between the measured pressure ratio and the mass flow rate of H_2, with a calculated Pearson correlation coefficient of 95.2×10^{-2} (n=48). Beyond this limit, the pressure response becomes insensitive to the parameters associated with fuel injection.

The figure also reveals a good agreement between part of the experimental data and the 0-D model. Such agreement may suggest that the experiments conducted under low equivalence ratio ($\varphi_G < 0.28$) have high combustion efficiency, or that the constant volume model is capable of estimating local temperature. However, it is important to notice that the simplified model does not account for the complex dynamics resulting from the supersonic interactions among flow, injection, and cavity. Local compressions, for instance, would lead to an increase in reactant pressure and consequently in products not included in the model. Therefore, further investigation is needed to support these observations.

4. Conclusion

This work investigated the relation between the pressure profile and the global fuel equivalence ratio in a hydrogen-fueled supersonic combustor directly connected to a shock tunnel. The results showed a direct correlation between combustion pressure ratio and fuel mass flow rate, for a constant air mass flow rate. Particularly noteworthy is the observation of a linear relationship for global equivalence ratios φ_G below approximately 0.25, indicating a combustion dynamic with linear dependency on φ_G and, consequently, on the fuel mass flow rate. This conclusion holds significant promise for simplifying models of supersonic combustion. However, as φ_G increases, the flow dynamics exhibited reduced sensitivity to changes in φ_G, posing a challenge for predictive modeling.

For fuel equivalence ratios above 0.28, measured pressures surpassed values calculated theoretically under the assumption of adiabatic combustion in a closed volume. This may have been caused by boundary layer separation as a result of excessive pressure increase with fuel injection.

Comparison of the experimental results to a 0-D model showed good agreement for equivalence ratios of 0.25 or below, suggesting that complete combustion occurs in such cases. Further investigation is required for confirmation.

Acknowledgements

This work was performed within the 'Technologies for Hypersonic Flights' project, coordinated by the Institute for Advanced Studies, is supported by the Brazilian Funding Agency for Studies and Projects (FINEP) under the Contract no.: 01.22.0255.00, by the Brazilian Air Force (COMAER) and by the Coordination for the Improvement of Higher Education Personnel (CAPES), under the Contract no.: PROCAD-DEFESA 88881.387753/2019-01.

References

1 Smart, M.: Scramjets. The Aeronautical Journal 111(1124), 605-619 (2007). https://doi.org/10.1017/S0001924000004796.

2 Curran, E.T.: Scramjet engines: the first forty years. Journal of Propulsion and Power, 17(6), 1138-1148 (2001). https://doi.org/10.2514/2.5875.

3 Liu, Q.: Cavity flameholding in an optical axisymmetric scramjet in Mach 4.5 flows. Proceedings of the combustion institute, 37(3), 3733-3740 (2019). https://doi.org/10.1016/j.proci.2018.08.037.

4 Yu, G.: Experimental investigation on flameholding mechanism and combustion performance in hydrogen-fueled supersonic combustors. Combustion Science and Technology, 174(3), 1-27 (2002). https://doi.org/10.1080/713712992.

5 Liu, Bing, et al.: Influence of Hydrogen Equivalence Ratios on Supersonic Combustion Based on Large Eddy Simulations. International Journal of Hydrogen Energy 45.19 (2020): 11341-11349. https://doi.org/10.1016/j.ijhydene.2020.02.054.

6 Kang, S. H.: Effects of flameholder configurations on combustion in scramjet engines. Journal of Propulsion and Power, 28(4), 739-746 (2012).

7 Lin, K. C.: Flame characteristics and fuel entrainment inside a cavity flame holder of a scramjet combustor. In 43rd AIAA/ASME/SAE/ASEE joint propulsion conference & exhibit, 5381 (2007). https://doi.org/ 10.2514/6.2007-5381.

8 Li, J.: Flame establishment and flameholding modes spontaneous transformation in kerosene axisymmetric supersonic combustor with a plasma igniter. Aerospace Science and Technology, 119, 107080 (2021). https://doi.org/10.1016/j.ast.2021.107080.

9 Cisneros-Garibay, E.: Flow and Combustion in a Supersonic Cavity Flameholder. AIAA journal, 60(8), 4566-4577 (2022). https://doi.org/10.2514/1.J061533.

10 Liu, Q.: Review of combustion stabilization for hypersonic airbreathing propulsion. Progress in Aerospace Sciences, 119, 100636 (2020). https://doi.org/10.1016/j.paerosci.2020.100636.

11 Cai, Z.: Review of cavity ignition in supersonic flows. Acta Astronautica, 165, 268-286 (2019). https://doi.org/10.1016/j.actaastro.2019.09.016.

12 Wang, Z.: Review of cavity-stabilized combustion for scramjet applications. Proceedings of the Institution of Mechanical Engineers, Part G: Journal of Aerospace Engineering, 228(14), 2718-2735 (2014). https://doi.org/10.1177/0954410014521172.

13 Chapuis, M., et al.: A computational study of the HyShot II combustor performance. Proceedings of the Combustion Institute 34.2 (2013): 2101-2109. http://dx.doi.org/10.1016/j.proci.2012.07.014.

14 Vialta, L.M. Estudo dos Efeitos de Cavidades Abertas em Combustores Supersônicos. PhD Thesis. Aeronautics Institute of Technology, Brazil (2023).

15 ANDERSON JR, J. D. Fundamentals of Aerodynamics. McGraw-Hill Series in Aeronautical and Aerospace Engineering. 3rd Edition, New York, NY, 2001.

16 Korkegi, R. H: Comparison of shock-induced two-and three-dimensional incipient turbulent seperation. AIAA journal, 13(4), 534-535 (1975). https://doi.org/10.2514/3.49750